Numerical simulations of fast ion loss measurements induced by magnetic islands in the ASDEX Upgrade tokamak

2009 Nucl. Fusion 49 095021

(http://iopscience.iop.org/0029-5515/49/9/095021)

IOP Publishing and International Atomic Energy Agency Nuclear Fusion
Nucl. Fusion **49** (2009) 095021 (14pp) doi:10.1088/0029-5515/49/9/095021

Numerical simulations of fast ion loss measurements induced by magnetic islands in the ASDEX Upgrade tokamak

M. Gobbin[1], L. Marrelli[1], H.U. Fahrbach[2], M. Garcia-Muñoz[2], S.Günter[2], P. Martin[1], R.B. White[3] and the ASDEX Upgrade Team

[1] Consorzio RFX, EURATOM-ENEA Association, Corso Stati Uniti, 4 - 35127 Padova, Italy
[2] Max-Planck-Institut für Plasmaphysik, EURATOM Association, Garching, Germany
[3] Princeton Plasma Physics Laboratory, Princeton, NJ, USA

Received 7 April 2009, accepted for publication 2 July 2009
Published 4 September 2009
Online at stacks.iop.org/NF/49/095021

Abstract
A test particle approach, implemented with the Hamiltonian code ORBIT, is used to simulate measurements of fast ion losses induced by magnetic islands in the ASDEX Upgrade tokamak. In particular, the numerical simulations reproduce the toroidal localization of losses and the lost ions pitch angle and energy distribution experimentally measured with the fast ion losses detector (FILD) in the presence of a neoclassical tearing mode (NTM). The simulated NTM induced losses occurring on time scales longer than 100 μs are composed of mainly trapped or barely passing particles, consistently with the slow decay of the experimental signal from one FILD channel after the beam switch-off. The numerical simulations have been performed by taking into account the D-shaped plasma geometry, the collision mechanisms, the losses due to ripple effects and the rotation of the mode. The radial profile of the magnetic perturbation is adjusted in order to match ECE measurements. While statistical properties of FILD measurements are rather well reproduced, the simulated total amount of losses is found to be significantly affected by edge details of the magnetic perturbation as it determines the loss mechanism.

PACS numbers: 52.55.s, 52.75.d, 52.50.b, 52.35.g, 52.25.Xz, 52.65.y, 52.55.Tn

(Some figures in this article are in colour only in the electronic version)

1. Introduction

Fast particles from neutral beam injection (NBI) and from radio frequency (RF) heating represent a significant fraction of particle population in present day magnetic fusion experiments. Fast particle dynamics is significantly different from that of thermal particles, especially for what concerns their interaction with the magnetohydrodynamics (MHD) instabilities. In particular, it has been experimentally shown that long wavelength modes negatively affect the transport and increase the losses of fast ions from NBI or RF [1, 2]. This is an important topic both for present day experiments and future reactors. In fact, the losses of high energy particles may diminish the efficiency of NBI heating and current drive; moreover, an intense and localized loss of fast ions may also damage the plasma facing components.

In order to study this important issue, an experimental investigation has been performed in the ASDEX Upgrade tokamak (AUG, major radius: 1.65 m, minor radii: 0.8 and 0.5 m) [3]. A fast ion losses detector (FILD) has been installed and initial results on the effect of MHD instabilities on fast particle losses were shown in [4, 5]. The FILD measures, in a given toroidal location, the flux of lost fast ions resolved in pitch angles and energy with high time resolution (1 MHz). Its design is based on the concept of the α particle detector used for the first time at TFTR [6, 7] and more recently in other fusion devices such as CHS [8], W7-AS [9], LHD [10], JET [11], NSTX [12] and TJ-II [13]. A more detailed description of it can be found in [4] with an overview of the first measurements. Fast ions enter through a slit and hit a scintillator plate, which is imaged with a CCD camera (with high spatial resolution) and with an array of 20 fast photomultiplier tubes. The strike points of the fast ions depend on their gyroradius (i.e. energy) and on the topology of their orbit. More precisely, they depend on their pitch λ, defined as $\lambda = \frac{v \cdot B}{vB}$, where v is the ion velocity and B the magnetic field.

The simulations discussed in this paper refer to experiments which have been performed in plasmas with

toroidal current $I_p = 0.8$ MA, toroidal field $B_t = 2$ T, safety factor at the edge $q_{95} = 4.5$ and NBI as fast deuteron source (reference discharge #21089 at $t = 4$ s). We focus in particular, on those plasmas where a (2, 1) neoclassical tearing mode (NTM) is present. Note that in these shots the NBI heating is co-current and the whole plasma is rotating in the current direction and so does the NTM [25].

The birth energy of the fast ions considered here is of 93 keV. As will be shown in section 2.4, the slowing down time scale due to collisions is much longer than the typical loss time, so the fast particles hit the FILD with energy very close to their initial one, in a range between 90 and 93 keV.

We summarize here the main experimental findings [4] that we are aiming to reproduce by the model described in this paper:

- The NTM increases the fast ion losses.
- The energy distribution of the lost ions at FILD location is mainly peaked at the injection energy (93 keV).
- The pitch distribution is not uniform but several distinct peaks may appear depending on the presence of the (2, 1) NTM mode. In particular, the measurements are characterized by two peaks at $\arccos(\lambda) \simeq 55^\circ$ and 70° when no NTM is present; another peak appears at $\arccos(\lambda) \simeq 40^\circ$ when the mode occurs.
- The amplitude of some of the peaks is modulated at the same frequency of the (2, 1) mode.
- Losses for certain classes of fast ions may occur on very long time scales (1–2 ms, see [4]), i.e. after a very high number of toroidal turns.

Some of these features were qualitatively interpreted by means of a simplified model [4], based on the integration of fast ions guiding centre orbits in a tokamak of cylindrical geometry and circular cross section, in the presence of a stationary (2, 1) perturbation of the magnetic field.

High energy particles are subject to a displacement of their orbit, proportional to their velocity and to the local value of the safety factor q (a generic analytic derivation is given in [14]). This shift of the particle orbits couples with the (2, 1) NTM mode and generates drift islands or stochasticity in the fast ion phase space, as will be described in section 2.1. In both cases toroidally localized losses may occur.

On the other hand, trapped fast ion losses are critically influenced by the presence of the magnetic field ripple due to the finite number of toroidal coils. Therefore, a more accurate simulation of FILD measurements requires the inclusion of the ripple effect. A comprehensive analysis of the collisionless fast ion losses mechanism in D-shaped geometry, with ripple and magnetic perturbation, is given in [15].

The aim of our paper is the reproduction of the final distributions characterizing the pitch angle, energy and toroidal angle of the lost ions in different scenarios. The investigation on the absolute amount of losses, and its direct comparison with the experiment, is beyond the scope of our work. Thus, the percentages of losses reported in this paper are only useful for comparing the different kinds of numerical simulations performed. An additional section is also dedicated to investigate the effect of different assumptions on the radial profile of the (2, 1) NTM eigenfunction. In fact, while the location and size of the (2, 1) island is rather well measured with the ECE and SXR diagnostic, detailed information on the precise shape of the mode eigenfunction is missing. We find that the choice of the magnetic perturbation profile has important consequences both on the dominant loss mechanism and on the actual loss rate. We will show that the magnetic perturbation details in a region near the edge are critical for determining the nature of the loss mechanism and the amount of losses.

The simulations that we are going to show here include both collisions and the rotation of the mode. The latter point is important because losses are observed also on long time scales, comparable to or longer than the rotation period.

The paper is organized as follows. In section 2 a description of the model that we use for the numerical simulations is presented. Then the main results of the simulations of FILD experimental data are reported both for a stationary and for a rotating perturbation in section 3. Section 4 deals with a sensitivity study on the effect of the perturbation profile on the simulated amount of losses. We conclude with a summary of the main results obtained.

2. Description of the fast ion losses model

Simulations are performed by integrating the trajectories of an ensemble of fast ions for a fixed amount of time. Particles hitting a prescribed loss surface are recorded as lost. Particles' trajectories are computed by means of the ORBIT code [16] that integrates the equations of motion in Hamiltonian form using flux coordinates. As losses occur near the separatrix, which is not well represented in Boozer coordinates, the ORBIT code has been upgraded in order to solve the equations of motion expressed in terms of generic straight field lines flux coordinates [17]. In its present version the ORBIT code only deals with flux coordinates which are well defined only up to the separatrix: therefore particles' trajectories cannot be integrated along open field lines, as is done in [15]. In the simulations described in this paper we consider as lost those particles whose trajectory hits a flux surface near the separatrix: as the particles could re-enter the separatrix without hitting the first wall, the absolute amount of losses may be overestimated, as discussed in section 3.1. This does not represent a significant limitation for our analysis since we are not interested in the absolute amount of fast ion losses but only in the final distributions features.

The flux coordinates which define the position of a particle are the angle along the toroidal direction (ζ), the poloidal angle θ and the poloidal magnetic flux ψ_p which labels the magnetic flux surfaces (where $\psi_p = 0$ is the magnetic axis). The components of the equilibrium magnetic field (both controvariant and covariant) are computed by the VMEC code [18].

2.1. Magnetic perturbation

An important result of the simulations that will be described in the following sections is that the amount of losses strongly depends on the details of the magnetic perturbation radial profile. Therefore, we recall here the method we used for modelling the mode radial eigenfunction. An analytical expression for the radial field profile b^r is assumed and a

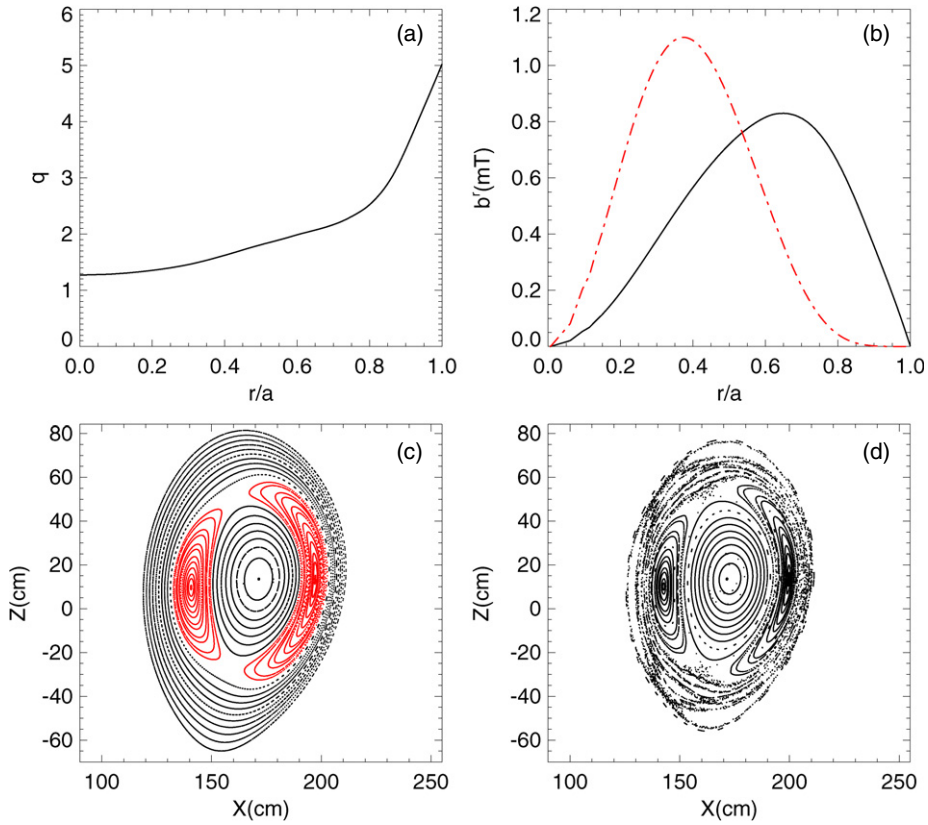

Figure 1. (*a*) Profile of the safety factor q for the AUG discharge 21089. (*b*) Two different parametrizations of the radial component of the magnetic field perturbation for the (2, 1) mode: the solid line refers to equation (2) and the dashed line to equation (12). (*c*) Poincaré map of a poloidal section by field line tracing with ORBIT. (*d*) Representation of fast ion 93 keV space phase.

multiplicative factor is adjusted in order to reproduce the size of a (2, 1) magnetic island on the low-field side as measured by the ECE diagnostic, which allows us to determine it with an accuracy of 2 cm. As no other information on the eigenfunction is available we have to rely on the analytical expression; we will discuss in section 4 the effect of different assumptions for the eigenfunctions profiles on fast ion losses.

A magnetic perturbation $\boldsymbol{b}_{m,n}$, associated with a MHD mode with poloidal and toroidal number m and n, respectively, is represented in the ORBIT equations in the following way:

$$\boldsymbol{b}_{m,n} = \nabla \times \alpha_{m,n}(\psi_\mathrm{p}) \sin(m\theta - n\zeta + \phi_0)\boldsymbol{B}, \qquad (1)$$

where $\boldsymbol{B}$ is the equilibrium magnetic field, ϕ_0 is the initial phase of the mode and $\alpha_{m,n}$ is a generic scalar function of the poloidal flux coordinate. We first consider the same expression of α also adopted for the simulations in [4]:

$$\alpha(\psi_\mathrm{p}) = \alpha_0 r(\psi_\mathrm{p})^m (\psi_\mathrm{p} - \psi_\mathrm{pw}). \qquad (2)$$

In this expression $r(\psi_\mathrm{p})$ is the radial distance from the magnetic axis along the equatorial plane normalized to the major radius R_0 and ψ_pw is the poloidal flux at the wall; in our case $(m, n) = (2, 1)$. By adjusting the constant α_0 it is possible to match the experimentally determined amplitude of the island: we chose for the simulation a width of 11 cm.

The safety factor q profile is shown in figure 1(*a*); the resonant position for the mode (2, 1) is at the radius $r/a \simeq 0.6$. In the same figure in (*b*) the solid curve is the profile of the radial component b^r corresponding to $\alpha(\psi_\mathrm{p})$ as given by equation (2). The topology of the magnetic field line, when such a perturbation of the magnetic field line is present, is shown in panel (*c*). This is performed with ORBIT field line tracing, i.e. following the guiding centre motion of very low energy particles with velocity parallel to the magnetic field lines. The magnetic perturbation only causes the formation of magnetic islands but no magnetic field line stochasticity.

The topology of passing fast ion orbits can be significantly different compared with the field line topology, as shown in figure 1(*d*) for fast ions with 93 keV energy. The points represent intersections of $\lambda = 1$ passing co-current fast ion orbits with a poloidal cross section. In fact, as observed in the introduction, high energy passing particle orbits are displaced by an amount proportional to their velocity and to the local value of the safety factor q [14]. When a mode is present, the orbits of particles deposited in regions near the displaced resonant surface are distorted and a (2, 1) island appears together with several other islands. In fact, the displacement of the orbit, which has a (1, 0) character, couples with the (2, 1) resulting in passing fast ion orbits with helicity (1, 1), (3, 1) and (4, 1), depending on their radial location: these trajectories define drift islands. Depending on the q profile, on the shape of the magnetic perturbation and on the fast ion orbital properties (energy and pitch angle) these islands may or may not overlap. In the former case, orbits become stochastic; therefore, high energy passing particles can follow perturbed trajectories which connect central regions of the plasma to the edge and finally to the first wall, increasing the loss rate of fast

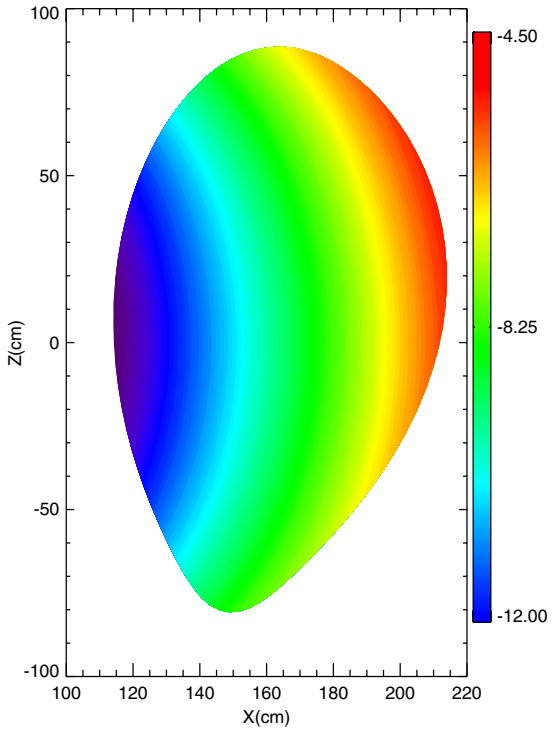

Figure 2. Ripple map of Asdex Upgrade. Contour colours refer to A (in logarithmic scale).

ions. The orbit stochasticity has already been considered in the past [19] to explain fast ion losses.

2.2. Ripple implementation

Simulations of fast ion losses also need to take into account other deviations of the magnetic field from axisymmetry. This is particularly true for trapped particles when a ripple of the toroidal field, due to the finite number of coils, is present. The guiding centre equations of motion implemented in ORBIT take into account the effect of the ripple. In particular, we used an analytical representation for the ripple perturbation R_p as follows:

$$R_\mathrm{p} = A(\psi_\mathrm{p}, \theta)\sin(N\zeta), \tag{3}$$

where N is the number of coils and A is the local amplitude of the ripple. Equation (3) is added to the magnetic field expression in the equations of motion in ORBIT. In AUG the ripple effect is described by the following equations:

$$\alpha_\mathrm{rip} = -21.959 + 4.653Z(\psi_\mathrm{p}, \theta)^2 + 1.747Z(\psi_\mathrm{p}, \theta)^4, \tag{4}$$

$$\beta_\mathrm{rip} = 7.891 - 1.07Z(\psi_\mathrm{p}, \theta)^2 - 0.86Z(\psi_\mathrm{p}, \theta)^4, \tag{5}$$

$$A(\psi_\mathrm{p}, \theta) = \exp(\alpha_\mathrm{rip} + \beta_\mathrm{rip}X(\psi_\mathrm{p}, \theta)), \tag{6}$$

where A is normalized to the on-axis field B_0 and X, Z are the usual Cartesian coordinates on a poloidal section [20]. In figure 2 a contour plot of $\log(A)$ is shown.

2.3. Distribution of injected particles

The initial test particle positions, energy and velocity are obtained by the FAFNER [21] code, which models the interaction between the neutral particles injected by the NBI system with an energy of 93 keV and the plasma background. The FAFNER code adopts a Monte Carlo approach and gives the initial positions for an arbitrary number of test particles. We have chosen 30 000 fast ions, as a compromise between the need to increase statistical accuracy and to reduce the computation time. All of the statistical indicators that will be presented in the paper are based on the number of particles with certain characteristics and will be expressed as a fraction of the number of initial ions.

The FAFNER code gives particle positions in cylindrical coordinates; therefore, a numerical conversion to flux coordinates is performed. Note that the conversion algorithm fails for a limited number of particles whose poloidal coordinate is around 0. These particles are not included in the simulations.

The FAFNER code gives the initial pitch λ of each particle. For comparison with FILD measurements, we shall use the pitch angle defined as $\arccos(\lambda)$, a quantity that directly gives the angle between the particle velocity and the magnetic field direction in degrees. A passing ion, whose velocity is aligned to the magnetic field is characterized by $|\lambda| = 1$ and pitch angle 0°, while a trapped ion with $|\lambda| = 0$ has a pitch angle of 90°.

The spatial and pitch angle fast ion distributions are reported in figures 3(a) and (b). The ions are initially distributed almost uniformly in the normalized radial coordinate r/a, with a maximum near the centre of the plasma.

Fast ions are injected both more radially (two NBI sources) and more tangentially (one NBI source). Their initial pitch angle distributions are plotted in figure 3(b) with a thin line (for the ions radially injected) and a thick black line (for ions tangentially injected). The two histograms are centred around a different maximum of pitch angle value. In particular, the radially injected ions distribution is mainly composed of trapped particles, with $\arccos(\lambda) \sim 70°$ while the other one includes both barely passing and trapped fast ions around $\arccos(\lambda) \sim 50°$.

A projection on a poloidal plane of the initial ions positions is given in figure 4 where the coloured points represent particles which are lost within 3 ms, a time comparable to the typical experimental loss time scale. The different colours correspond to different initial pitch angle λ values. In particular, the NTM will be shown to mainly affect particles plotted with green dots. Few of these ions are very close to the loss surface and are lost also without the mode in a very short time (less than 10 μs) because of their high energy drift (first orbit losses). Particles deposited in the region between the loss surface and the first wall (amounting to 1.6%) are not considered in the simulations. In fact, we have set a minimum loss time of 0.1 μs so that these ions are not taken into account in the final statistics. All particles lost within 3 ms were originated in an outer region of the plasma, not far more than 5–8 cm from the edge.

2.4. Collision mechanisms

For completeness, the numerical simulations include collisions with the thermal plasma background. Particles are, in fact, subject to pitch angle scattering [22] and slowing down

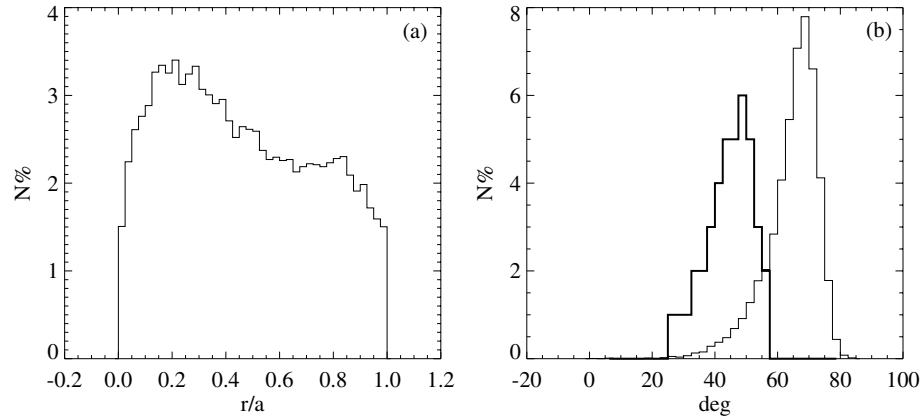

Figure 3. (*a*) Initial distribution of the fast ions 93 keV deposited from NBI. (*b*) Initial pitch angle distributions for radially (thin line) and tangentially (thick line) injected ions.

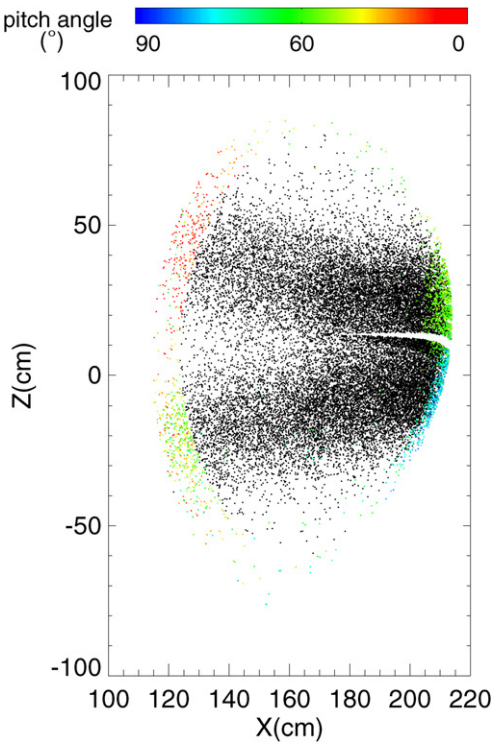

Figure 4. Map of the initial position of the particles from NBI projected on the poloidal cross section. The coloured particles are those lost within 3 ms; different colours correspond to different initial pitch angles.

collisions [23] with both the thermal ions and the electrons of the background. While the pitch angle scattering mechanism is related to transverse diffusion and changes the direction of the fast ions velocity, the slowing down is responsible for their thermalization.

Typical pitch angle collision frequencies for a ∼100 keV fast ion with background ions with energy of a few kiloelectronvolts are in the range: $\nu_d \sim 3$–15 Hz. A similar estimate performed considering the fast ions interaction with a background of thermal electrons with energy of a few kiloelectronvolts gives a collision frequency about two orders of magnitude lower and is therefore neglected.

The slowing down collision frequency for a 100 keV fast ion is one-half of the corresponding pitch angle collision frequency: $\nu_s \sim 1$–10 Hz; thus the time required by a fast ion to decrease its energy by a factor 1/3 is $\tau_s \sim 80$–200 ms.

2.5. *Implementation of a rotating mode*

Simulations have been performed including the rotation of the mode. This may be important as there is experimental evidence that fast particles may also be lost on time scales comparable to the rotation period. This means that the phase of the mode changes considerably during the dynamics of these particles.

First of all, when the mode rotates, an electrostatic potential needs to be introduced to compensate the electric field induced by the magnetic flux variation so that the simulation is performed with a net zero electric field parallel to $\boldsymbol{B}$: the origin of the zero field constraint is due to the fact that the background electrons rapidly short out the field induced by the magnetic flux time variation.

More precisely, let us consider a time dependent version of equation (2):

$$\alpha(\psi_p, \theta, \zeta, t) = \tilde{\alpha}(\psi_p)\sin(m\theta - n\zeta + \omega t), \tag{7}$$

which becomes equation (2) assuming $\tilde{\alpha}(\psi_p) = \alpha_0 r(\psi_p)^m(\psi_p - \psi_{pw})$ and $\omega = 0$. In the case $\omega \neq 0$ the time variation induces an electric field that needs to be shorted out by the ad hoc introduction in the code of an electrostatic potential with the following form

$$\Phi = \tilde{\Phi}(\psi_p)\sin(m\theta - n\zeta + \omega t). \tag{8}$$

The required expression for $\tilde{\Phi}$ is obtained by the Maxwell equation: $\nabla \times \boldsymbol{E} = -\partial_t \boldsymbol{B}$ applied to the perturbation of magnetic field $\delta\boldsymbol{B}$ which has a vector potential $\delta A = \alpha B + \nabla\Phi$ (gauge's choice). Using equation (1) we have

$$\boldsymbol{E} = -\frac{\partial(\alpha\boldsymbol{B})}{\partial t} - \nabla\Phi = \omega\alpha\boldsymbol{B} - \nabla\Phi. \tag{9}$$

But the rapid mobility of electrons shorts out the parallel electric field $E_{||}$ on a very fast time scale, thus,

$$E_{||} = \omega\alpha B - \boldsymbol{B}\cdot\nabla\Phi/B = 0. \tag{10}$$

By expressing the differential operators in straight field lines coordinates, we finally obtain an approximated relation defining the electric potential:

$$\tilde{\Phi} = \omega\tilde{\alpha}\frac{\langle JB^2\rangle_\theta}{nq-m}, \tag{11}$$

where $\langle\ldots\rangle_\theta$ represents the average over θ and J is the Jacobian.

Note that equation (11) diverges towards the magnetic island O-point where $q \to m/n$. Such an unphysical behaviour is regularized by replacing $(nq-m)^{-1}$ with $(nq-m)/((nq-m)^2+(\Delta)^2)$ where Δ is a small positive term which equals the quantity $(nq-m)$ evaluated at the island separatrix. The effect of this regularization term is negligible outside the magnetic island, since $\Delta \ll (nq-m)$. Since the lost fast ions come from a region outside the magnetic island, near the edge of the plasma, this artificial regularization does not affect the dynamic and the results of our simulations.

3. Fast ion losses simulations

In all simulations, whose results are being presented to explain FILD measurements, the ORBIT code is used to integrate the trajectories of fast ions subject to the magnetic perturbation described in equation (2). The magnetic field ripple, as described in section 2.2, is always included, as it is an important loss mechanism for trapped particles.

The magnetic perturbation due to the (2, 1) NTM, which is described by equation (2), can be either stationary or rotating. In the latter case an electrostatic potential, as shown in the previous section, is added. Finally, the code runs can be performed in *burst mode* or in *steady state*. In the former case, the integration of an initial ensemble of particles is performed for a finite amount of time (typically 3 ms): once a particle reaches a prescribed loss surface, it is not considered anymore. Steady-state simulations are performed by keeping constant the number of particles during the simulation time: when a fast ion reaches the loss surface, a new one, chosen randomly from the particles distribution generated by the code FAFNER, is reintroduced in the plasma.

In summary, the following kinds of simulations have been performed and will be described in the following:

- *A stationary NTM*. The simulations are performed in burst mode, with and without a (2, 1) NTM. The main finding is that the NTM significantly affects the amount of fast ion losses and their statistical distributions.
- B *Steady state, rotating NTM*. In stationary simulations fast particles may be lost on time scales comparable to the NTM rotation period. Steady-state simulations with a rotating NTM confirm the statistical distributions simulated in the stationary case.
- C *Burst mode, rotating NTM*. This kind of simulation is performed to simulate experimental behaviour of losses in modulated beam experiments. In particular, the simulation aims at justifying the time behaviour of different classes of fast ions, immediately after the switch off of the beams.

3.1. Stationary perturbation

The presence of the NTM significantly affects the overall amount of losses. After 3 ms, in fact, about 10% of the 93 keV fast ions is lost when a stationary (2, 1) mode is included in the simulation. On the other hand, only 7% of fast ions is lost when the NTM is not present. The statistical fluctuation due to the finite number of particles chosen for the simulations amounts to ∼0.2%: we verified, in fact, that the estimate of losses approximately follows Poisson statistics. This has been done by extracting several random samples of the initial population of fast ions and evaluating the distribution of the total amount of losses. As this source of uncertainty is negligible compared with other assumptions in the simulations we dropped errors in all subsequent discussion.

While the increase in losses due to the NTM is statistically significant, the simulations cannot be used to predict the absolute value of the losses, because of the distance between the loss surface, which is necessarily located inside the separatrix, and the first wall. As an example, if the loss surface is set 3.3 cm away from the separatrix, NTM induced losses with a stationary perturbation grow to 18%. It is therefore very likely that losses predicted by the ORBIT code are overestimating the experimental losses. Nevertheless, despite the limitation of the model, the statistical properties of the losses do not change significantly in the two simulations and explain rather well FILD measurements.

The radial profile of the mode amplitude is the one described by equation (2) and the phase of the NTM mode (2, 1) has been changed to different values in order to verify the experimental behaviour, i.e. to check whether the particles losses are in phase with the mode.

3.1.1. Toroidal distribution of losses. Not only the absolute value of fast ion losses but also their statistical distributions are affected by the NTM. Let us first analyse the pitch angle of the lost particles and the position where they reach the loss surface. The final toroidal and poloidal angles for the lost ions are plotted in figure 5 for two different cases: without (*a*) and with (*b*) the NTM perturbation. The different colours in figure 5 refer to the final pitch angle of the particles. When no NTM is present in the simulation, the losses are almost uniform in the toroidal direction. As far as the poloidal distribution is concerned, low pitch angle (i.e. passing) ions are distributed over a wider θ region, compared with high pitch angle ions. The latter class of lost ions include barely passing (green) and trapped (cyan-blue) particles.

When a stationary (2, 1) mode is included in the simulation, the fraction of lost particles with pitch angle in the range $\arccos(\lambda) = 60°$–$50°$ increases. Moreover, a large toroidally localized spot appears at (ζ, θ) near the poloidal plane $\theta = 0$, the region where the FILD detector lies. Such a spot, dominated by green dots, corresponds mainly to fast ion losses induced by the (2, 1) mode. The NTM also affects higher pitch angle particles, i.e. trapped particles, as shown by the blue-cyan spot in figure 5(*b*). Therefore, the NTM increases the losses of several classes of particles.

The toroidal localization of the losses is consistent with the observed experimental correlation between the phase of the mode and the losses. We have investigated this point

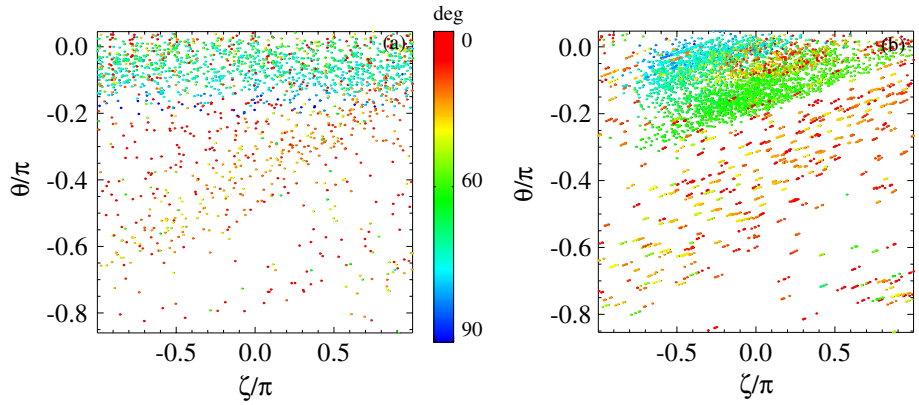

Figure 5. Final ζ and θ position of lost fast ions without (a) and with (b) the (2, 1) mode. The colour refers to the pitch angle.

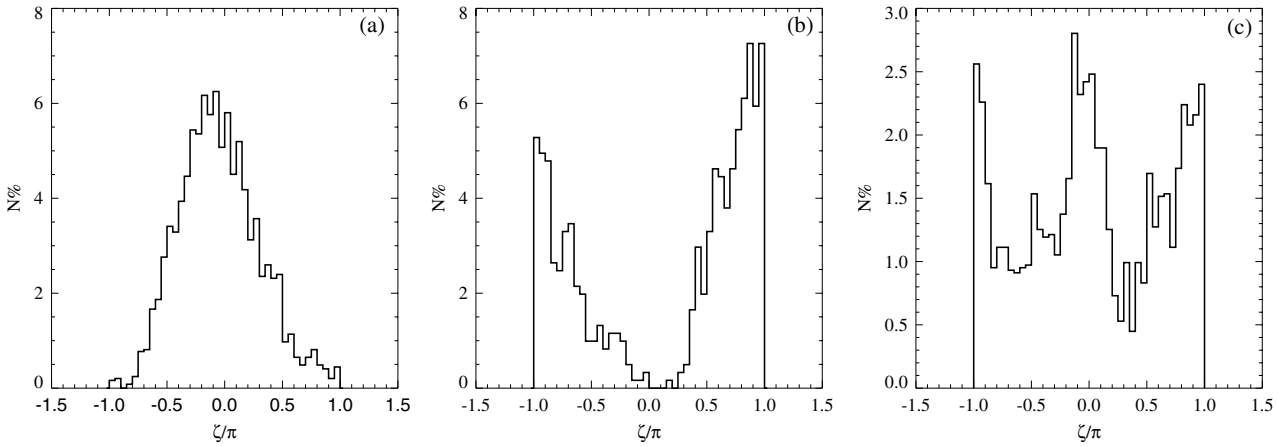

Figure 6. The toroidal localization of the losses depends on the phase of the mode. In (a) and (b) the phases of a (2, 1) NTM were shifted of π. In (c) the simulation has been performed with a (3, 2) NTM, and in the toroidal distribution two maxima appear.

by choosing different phases of the NTM and computing the final toroidal angle losses distribution after the simulations, as reported in figures 6(a) and (b). More precisely, the same figure shows the final toroidal angle distribution for the lost ions with pitch angle in the range: $\arccos(\lambda) \simeq 40^\circ$–$50^\circ$, i.e. for particles mainly lost when the tearing mode is present. The phase of the mode for the distribution in (b) is displaced by an angle of π with respect to the case of (a); correspondingly the maximum of the ζ distribution is moved by the same angle. The presence of a single peak in the final distribution reflects the toroidal character $n = 1$ of the mode (2, 1). Similar analysis for a (3, 2) mode are, in fact, characterized by two maxima, which move with the phase of the mode: an example of this is reported in figure 6(c).

3.1.2. Energy distribution. The energy distribution of lost ions is shown in figure 7(b). Most of the losses have a final energy around 93 keV, while only a small fraction, about 1%, is below 90 keV. This is in good agreement with the experimental data where fast ion losses have a final energy very close to their birth energy, i.e. 93 keV. This is due to the relatively long slowing down time (as stated above, of the order of 80 ms) compared with the loss time scales considered (1–3 ms); therefore, collisions play a negligible role.

3.1.3. Loss times distribution. Fast ion losses shown in previous figures occur at different time scales. This is highlighted by the analysis of the integral probability distribution of loss times, as reported in figure 7(a), neglecting the spatial localization of the losses. For a given time on the x-axis, the curve shows the fraction of the particles lost within that time both without (dashed line) and with (solid line) the NTM. The value of 100% represents all of the fast ions lost within 3 ms when the NTM is included in the simulation.

An amount of 20% of fast ion losses occurs on a very fast time scale (10 μs) and does not significantly depend on the NTM presence. These losses correspond to ions that cover a short distance, since a complete toroidal transit of the device requires about 3 μs. Most of these promptly lost ions were deposited on the high-field side and crossed readily on the low-field side due to the torus drift displacement of their orbits. The remaining fraction of lost fast ions population takes at least 50 μs to escape and is influenced by the NTM: without NTM, in fact, losses are smaller by about 35–40%.

Let us compare the toroidal localization of losses with and without NTM, distinguishing particles according to their loss time (figure 8). In plot 8(a) we report the toroidal and poloidal angles for the lost fast ions without the mode, thus only with the equilibrium magnetic field and ripple. The colour encodes the loss time with a logarithmic scale. Fast

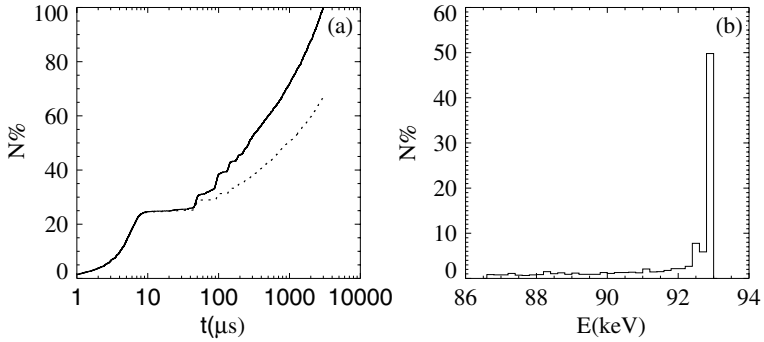

Figure 7. (*a*) Losses as a function of time in the first 3 ms of the simulation with (solid line) and without (dashed) the (2, 1) NTM. (*b*) Final energy distribution of lost ions (within 3 ms).

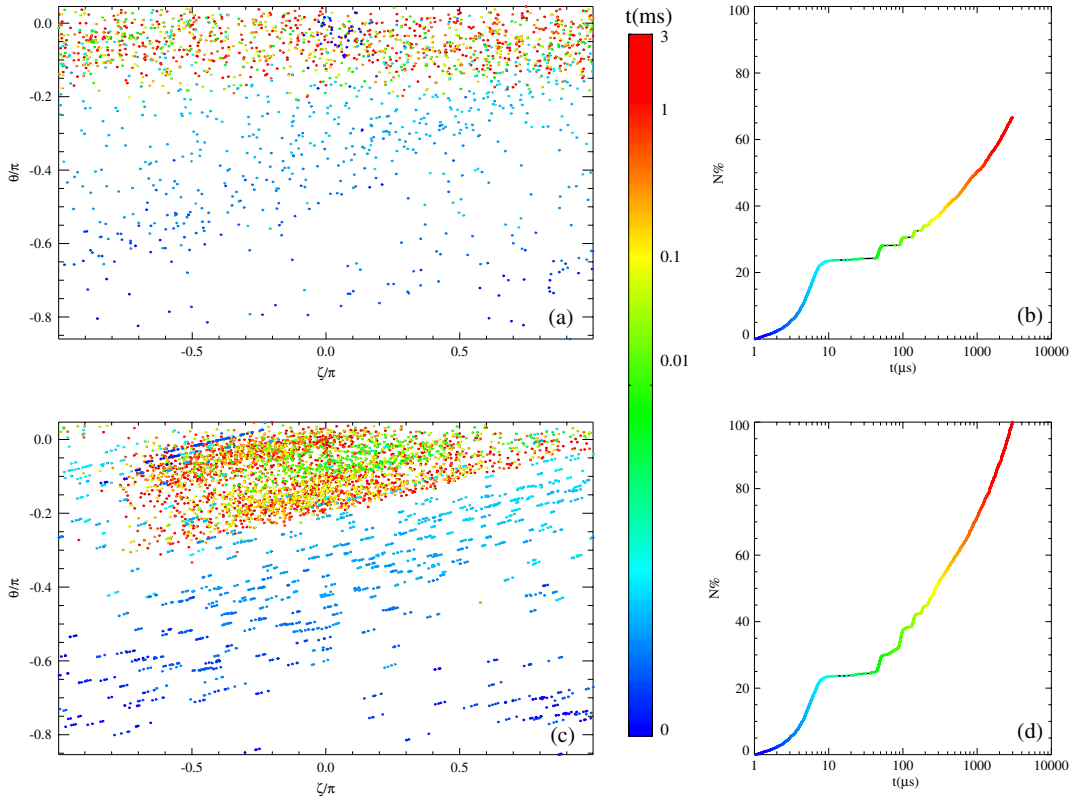

Figure 8. (*a*) Toroidal and poloidal distribution of lost ions without perturbation with colours corresponding to different time scales. (*b*) Cumulative time distribution of ions lost without perturbation. The 100% corresponds to the total amount of particles lost with the stationary mode (2, 1) within 3 ms (*c*) Toroidal and poloidal distribution of lost ions with perturbation with colours corresponding to different time scales. (*d*) Cumulative time distribution of ions lost with perturbation.

particles lost on longer time scales (orange and red points) are distributed uniformly. In contrast, when a stationary NTM is included in the simulation (figure 8(*c*)), not only do losses on long time scales increase but also they are concentrated in regions correlated with the phase of the mode. Therefore, the NTM influences the flux of fast particles in two ways: at first it increases the losses and secondly it concentrates them on a smaller area.

3.1.4. Pitch angle distribution. As recalled in the introduction, the pitch angle resolved measurements of 93 keV fast particles are characterized by the presence of two peaks when no NTM is present and by three peaks when the mode occurs (see [4]). Differently from earlier simulations based on a simplified circular geometry [4] and without the ripple of the toroidal field, now the simulations allow for a better comparison of the pitch angle distribution with the experimental data.

The distribution of pitch angle for lost ions around the midplane $\theta = 0$ ($-20^\circ < \theta < +20^\circ$), where the FILD lies, is shown in figure 9 both with (thin line) and without the NTM (thick line). In order to ease the comparison, the distributions have been normalized to the total number of lost ions. Two distinct peaks appear in the simulation when the mode is present while only one peak appears at 70° without the perturbation. This latter peak is mainly related to trapped particles, whose losses are due to the ripple of

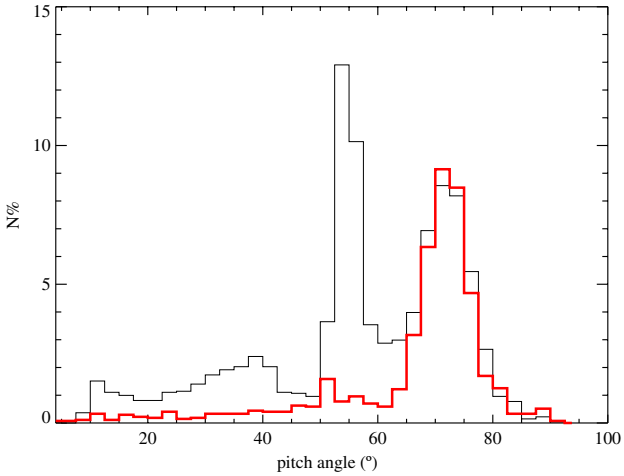

Figure 9. Final pitch angle distribution of the lost ions around the plane $\theta = 0$: the histogram with a thin line corresponds to the case with the perturbation (2, 1), the one with a thick line refers to the equilibrium scenario without the mode.

the magnetic field. Simulations performed without the ripple still show a peak at 70° but with a maximum value of 7% instead of 10%. The NTM does not affect this peak while it consistently increases losses of barely trapped fast ions around 55°. Moreover, a statistically significant enhancement of losses also occurs for barely passing particles, at 40°, corresponding to an experimentally observed peak by the FILD.

This characteristic pattern of losses depends on the relative distance between NBI sources and the FILD detector, and on the location and velocity direction of the fast ions. In particular, fast ions lost with $\arccos(\lambda) \sim 70°$ degrees are injected mainly radially (thin-line distribution in figure 3(*b*)), while those barely trapped (55°) and barely passing (40°) come from a tangential source (thick-line distribution in figure 3(*b*)).

3.2. Rotating perturbation

As a significant fraction of particles is lost on time scales of a few milliseconds, which is comparable to the rotation period of the (2, 1) mode, the assumption of a stationary perturbation may lead to systematic errors in the estimate of the losses. Steady-state simulations have been performed and the statistical properties of all particles lost during the run time have been gathered. The number of fast ions is kept constant during the simulation by generating a new particle, belonging to the initial distribution generated by the code FAFNER, every time a fast ion reaches the loss surface. Thus, the number of lost particles in steady state increases with the run time, differently from what happens in burst mode: we therefore compare the distributions obtained in the two scenarios by normalizing them to the actual number of particles lost in both cases. We have verified that, for the steady state, results do not depend on the run length.

Because of mode rotation, the toroidal angle distribution of the lost ions is uniform, as shown in figure 10(*a*). But this does not mean that the NTM is not playing a role in modifying the losses of fast ions. The toroidal angle distribution of lost ions is indeed modified in the reference frame where the (2, 1) mode is stationary. For each lost particle we define the new variable $\phi = \zeta - \omega t - \Phi_{in}$, where ζ is the final toroidal angle, t is the time at which the ion escapes the plasma and Φ_{in} is the initial phase of the mode. The quantity ωt is thus the phase of the mode when a particle is lost. The final distribution in the new variable ϕ is shown with a thick line in figure 10(*b*) which is very similar to that of a single burst run with a stationary mode (figure 6). To highlight this point we have reported on the same figure also the final distribution for the stationary mode (thin line), where $\phi = \zeta - \Phi_{in}$ since in this case $\omega = 0$.

Both simulations with and without the rotation of the mode, in a D-shaped geometry with ripple effects, confirm and partially improve the agreement with experimental data compared with the previous qualitative studies reported in [4] for a circular geometry approximation without ripple. The comparison is performed by mapping the time axis of the signal into the toroidal angle, assuming a rotation with constant angular velocity during one period and adjusting the initial phase to match the maximum of the toroidal angle distribution, as shown in figure 11. The experimental signal is in black and the simulation by ORBIT in red. In order to compare the two signals, only a multiplicative constant has been used to match the amplitude of the signal with the toroidal distribution.

The pitch angle distributions are similar for simulations with a rotating and a stationary (2, 1) mode. We have reported both of them in figure 12(*a*). Each curve represents the fraction of particles lost in a given pitch angle range normalized to the total number of losses during a simulation of 3 ms. The enhancement of losses at $\arccos(\lambda) < 45°$, $\arccos(\lambda) \sim 55°$ and $\arccos(\lambda) \sim 70°$ is clearly visible also for the rotating mode (thin line). The slight increase in trapped ions (peak at 70°) could be consistent with the resonance mechanisms between the mode rotation and fast ions toroidal precession/bounce frequency, as described in [24]. However, a detailed study on this issue is beyond the scope of our work.

3.3. Losses after beam switch-off

It has been reported in [4] that when the beam is turned off, the signal of different FILD channels decays with different time constants. Every FILD channel measures the flux of particles whose pitch angles are in a narrow range. While losses of particles at a pitch angle ≈40° (i.e. almost passing) decrease rapidly, fast particles with a pitch angle greater than ≈50° (i.e. trapped or marginally passing) can be detected for several milliseconds after the beam switch-off.

The model has therefore been applied to compare the time scales of particles losses with different pitches in order to simulate the behaviour of FILD measurements after a beam switch-off. Particles are not re-injected if they reach the loss surface; therefore, simulations are performed in burst mode. Distributions of loss times are shown in figure 12(*b*) for two classes of pitch angles. Particles with pitch angle in the range 65°–75° are lost on long time scales, up to 2–3 ms consistently with the observed slow decay of FILD signals, while lower pitch angle (i.e. 35°–45°) passing particles are lost on shorter time scales, up to 100 μs.

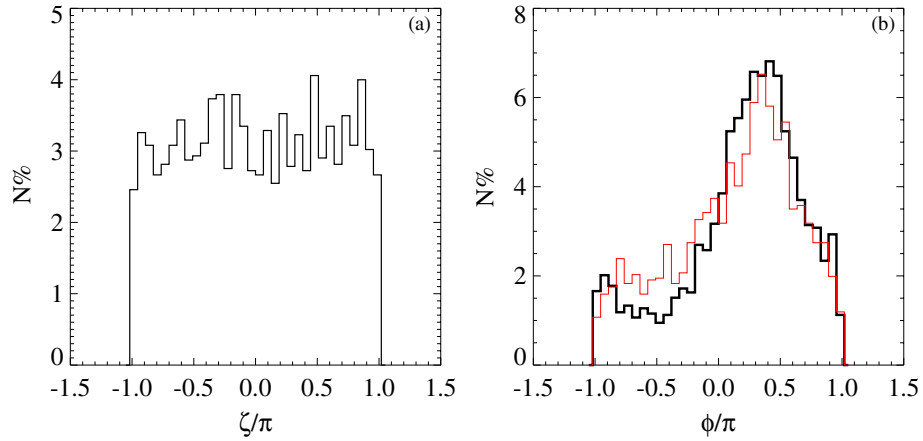

Figure 10. (*a*) In black the final toroidal angle ζ distribution of the losses when a rotating perturbation 5 kHz is present. (*b*) Final losses distribution in the new variable ϕ with a rotating (thick line) and a stationary (thin line) mode.

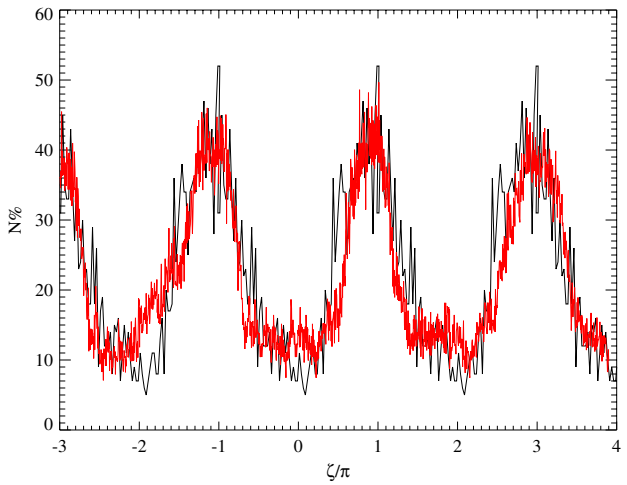

Figure 11. Experimental (black) and simulation (red) signal of the losses.

4. Effect of the radial perturbation profile on fast ion losses

The results shown in previous sections depend on the assumption on the magnetic field profile perturbation. As described in section 2.1, the ECE diagnostic was used to determine the island size; then, an analytical perturbation profile was multiplied by a constant in order to match this quantity. We illustrate here the effect of different assumptions: in particular, the effect of a different analytical profile and of the derivative of the eigenfunction near the (3, 1) resonance.

As presented in the following, while the fraction of lost particles depends on the eigenfunction profile assumed, on the other hand, the statistical properties of the final distributions are almost unchanged. The main conclusion is that, in order to better simulate fast ion losses, it is important to independently characterize the magnetic perturbation profiles in the edge region.

Following this section we describe numerical simulations without and with stationary NTM mode in burst mode. In the simulations we will compare three different classes of radial profiles.

In figure 13 we report Poincaré plots in the fast ion phase space, generated by the perturbation in equation (2) (panel (*a*)) and by a different α profile (panel (*b*)) of the form

$$\alpha(r,\theta,\zeta) = \alpha_0 \left(\frac{r(\psi_p)}{x_0}\right)^m \left(\frac{1-r}{1-x_0}\right)^{m(x_0^{-1}-1)} \times \sin(m\theta - n\zeta + \phi_0). \tag{12}$$

The free parameter x_0 allows us to adjust the position of the O-point, keeping the same island size. We show in figure 1(*b*) the b^r profile corresponding to equation (12), in a case with the O-point displaced by about 2 cm with respect to the location obtained with equation (2); the island width is always of 11 cm. The topology of fast ion orbits is significantly altered: the relatively small displacement of the (2, 1) O-point is such that drift islands do not overlap and chaos does not occur. With such a parametrization of the radial perturbation, fast ions reaching the loss surface within 3 ms amount to 7.5% of the particles initially considered in the simulation to be compared with 7% without perturbation, as already stated in section 3.1. This is barely greater than the estimated statistical fluctuation. On the other hand, approximately 10% of the initial fast ions population is lost when a perturbation such as equation (2) is assumed. This difference is due to the fact that particle orbits are deformed in a different way: if equation (12) is assumed, drift islands are smaller and do not overlap; therefore, orbits are less stochastic compared with equation (2).

We may, at first glance, expect that by increasing the mode amplitude, also drift islands would grow and eventually overlap. This would mean that orbit stochasticity would always occur above some threshold, whose exact value depends on the details of the eigenfunction, but the simulations we have performed do not confirm this picture.

To investigate this issue several simulations have been performed with increasing amplitude perturbation: simulated total losses have been plotted against the normalized magnetic fluctuation amplitude in figure 14. The thin curve corresponds to the perturbation described by equation (12) while the thick to the standard perturbation equation (2). The two families of perturbation profiles induce different fast ion losses at

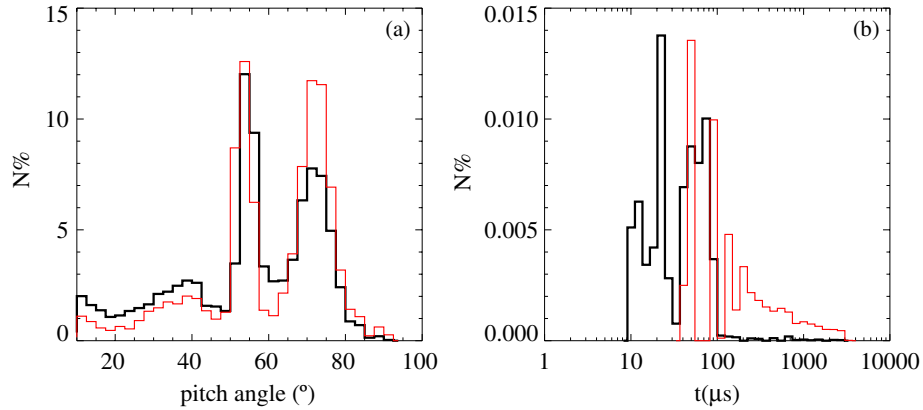

Figure 12. (*a*) Pitch angle final distributions: comparison between a stationary (thick line) and a rotating (thin line) perturbation. (*b*) Loss times distribution for different pitch angles ranges: the thin curve refers to pitch around 70; the thick one to pitch around 55. In (*b*) the axes are in logarithmic scales.

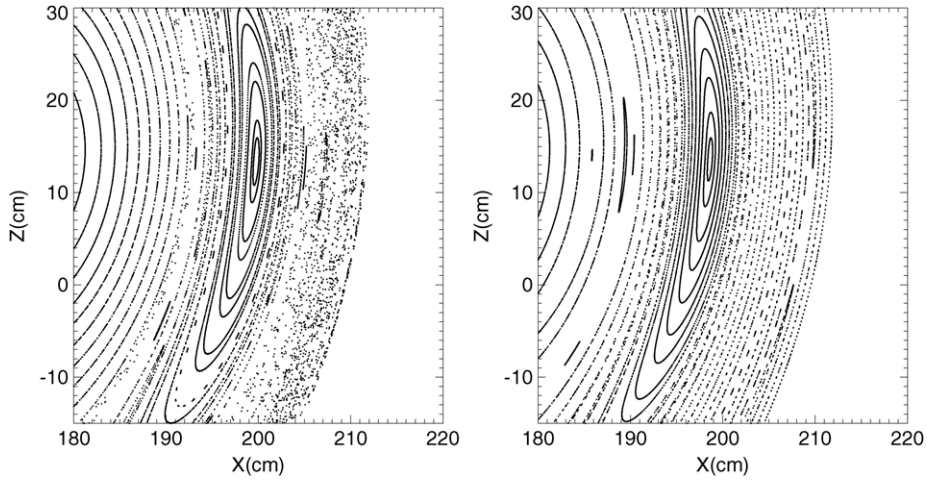

Figure 13. Right-hand side: zoom of the magnetic island obtained by a perturbation of the form equation (12). On the left: zoom of the magnetic island by equation (2).

all amplitudes of the magnetic perturbation. While at low amplitudes both types of perturbations produce few losses, a greater difference is observed at higher values. For the perturbation associated with equation (12) (diamonds) losses never increase above 20%, while for the other kind of profile a threshold occurs around $b^r/B_0 \simeq 0.1$–0.2% and values as high as 80% are reached.

An explanation of such a difference can be understood by considering in figure 15(*a*) the fast ion phase space puncture plot obtained by using equation (12) for a mode amplitude corresponding to an island size of 11 cm ($b^r/B_0 \sim 0.05\%$), such as the one of the experiment. This plot must be compared with the one obtained by using equation (2), which shows a clear increase in the chaotic domain especially near the edge. Therefore, for the same magnetic island size, the presence of stochasticity in the orbits reaching the loss surface depends critically on the details of the eigenfunctions in the edge region. At higher values of the mode amplitude (increased by a factor 4) orbits are stochastic with both parametrizations but with an important difference. Only the parametrization of equation (2) is such that stochastic orbits reach the loss surface. The plot in figure 15(*c*) refers to the perturbation given by equation (12) while (*d*) to equation (2). It is clear

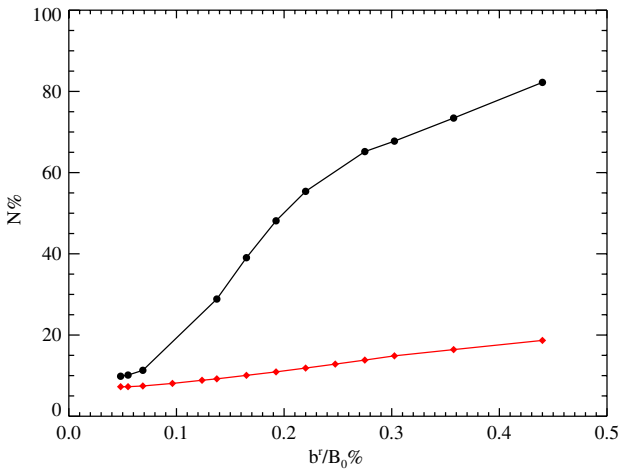

Figure 14. Percentage of losses as a function of the magnetic perturbation amplitude for equation (12) (diamonds) and equation (2) (dots).

how in the former case, although in the centre a high level of chaos is present, the orbit of passing fast ions near the edge are not stochastic. In contrast, the plot in (*d*) shows the presence of stochasticity over the entire plasma cross section and explains

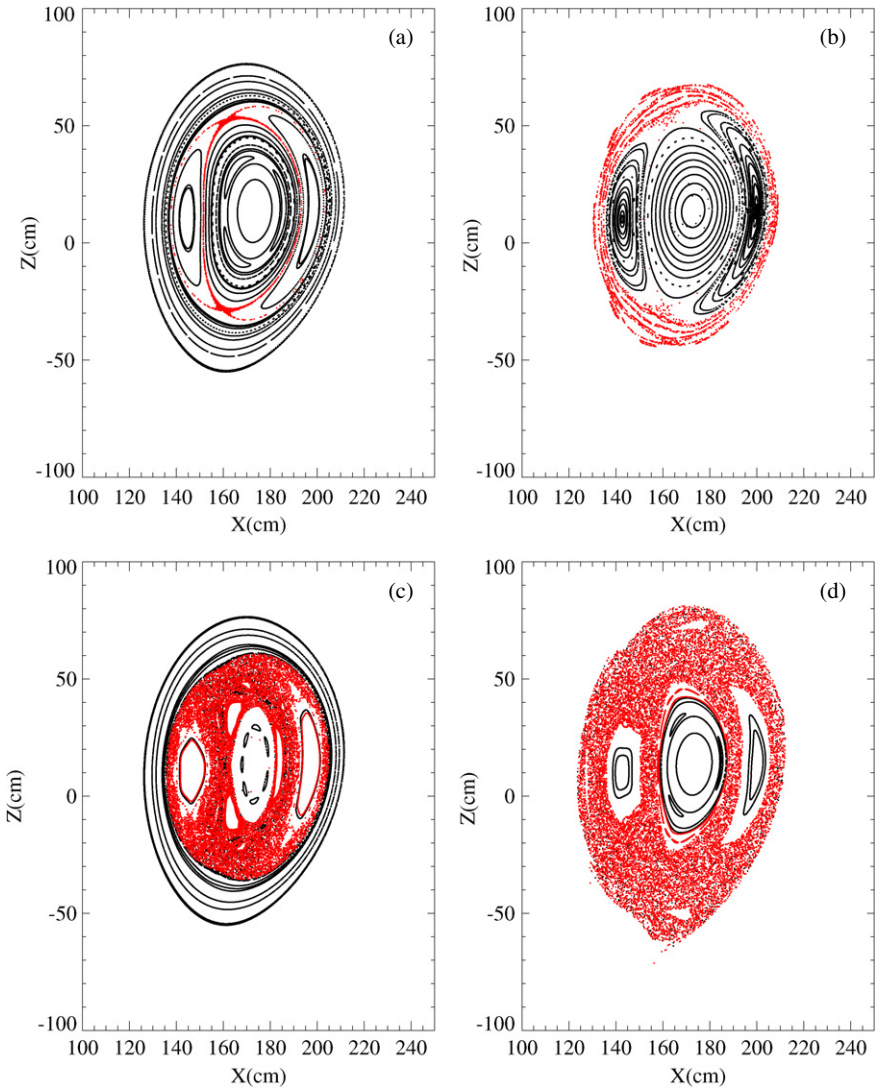

Figure 15. Comparison between the fast ion orbit puncture plots obtained by using equations (12)(*a*)–(*c*) (with $b^r/B_0 \sim 0.05\%$) and equations (2)(*b*)–(*d*) at different amplitudes ($b^r/B_0 \sim 0.2\%$) of the mode (2,1).

why about 80% of the initial fast ion population is lost at this large amplitude of the magnetic island.

The different effects of the two eigenfunction profiles on stochasticity in the fast ion phase space is explained by the different sizes of the islands chain generated by the coupling between the (2, 1) NTM and the (1, 0) high energy ions drift. Not only does the absolute value of the eigenfunction matter for the drift islands size but also its derivative.

In fact, for the eigenfunction profile of equation (2) (thick curve in figures 1(*b*)) both the value of the eigenfunction 2 and its derivative are significantly different from zero at the (3, 1) resonance radius (located at $r/a \approx 0.8$). Consequently, a large (3, 1) island characterizes the fast ion orbits (figure 15(*b*)). In contrast, for the profiles given by equation (12) (dashed line in figure 1(*b*)) the eigenfunction is very close to zero, resulting in a very small (3, 1) island.

In order to highlight the effect of the derivative of the eigenfunction we have locally modified the profile of equation (12) by adding a bump of magnetic perturbation $\delta\alpha$ centred close to the (3, 1) resonance position, defined as

$$\delta\alpha(r) = \frac{\alpha_1}{1+\gamma(|r-r_1|/a)^2}, \tag{13}$$

where α_1 is the amplitude of the bump at $r = r_1$, and γ determines its width. A plot of $\delta\alpha$ is reported in figure 16(*a*) with a dashed line, which, summed up to the profile of the basic eigenfunction (thick line) α in equation (12), gives the curve with a thin line . We have chosen as r_1 a radial position just before the resonance (3, 1), so as to have a non-zero derivative of $\delta\alpha$ at $r/a \simeq 0.8$. The corresponding eigenfunction for the magnetic perturbation b^r is reported in figure 16(*b*). Note that such an eigenfunction is consistent with a (2, 1) island size of 11 cm and therefore is not distinguishable from equation (12) on the basis of ECE data. Repeating the simulations, with this arbitrarily chosen correction of the (2, 1) eigenfunction radial profile, fast ion losses amount to 9%. Thus, by increasing the amplitude of the bump, in a region close to the drift island (3, 1) resonance condition, the lost ion fraction can increase considerably.

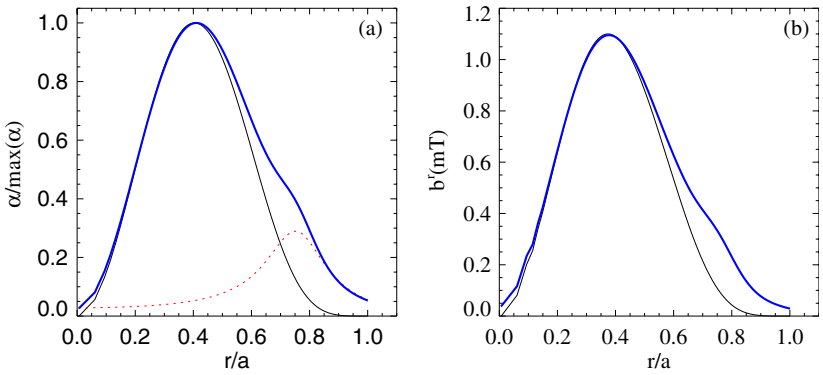

Figure 16. On the left: α function profile of equation (12) (thick line); the bump of equation (13) (dashed line) at the resonance (3, 1). The final profile obtained adding equations (13) and (12) with a thin line. On the right: the corresponding profiles for the magnetic perturbations.

It is worth noting that despite the choice of eigenfunction, i.e. equations (2), (12) or equations (12) + (13), the final toroidal angle and pitch angle distributions have the same features as those described for the cases discussed in the previous section; therefore, they cannot be discriminated by uncalibrated measurements of fast ion losses. The main difference in the three cases is the amount of losses due to the mode, which strongly decreases when considering the eigenfunction described by equation (12).

In summary this section has shown that the shape of the eigenfunction in the edge region can significantly affect total losses.

5. Summary

The ORBIT code, integrating fast particles trajectories in flux coordinates, has been modified to simulate experimental measurements by the FILD in ASDEX Upgrade. Even if particle orbits can be integrated only up to the separatrix and not to the first wall, several features of the experimental measurements of fast ion losses have been reproduced by accurate numerical simulations and confirmed earlier results obtained with simpler simulations.

The presence of an NTM not only increases the total amount of losses but also concentrates the fluxes on smaller areas, whose location is correlated with the mode phase. The position of the lost fast particles depends on the mode phase at the time at which the particle reaches the loss surface.

A more realistic D-shaped geometry and the inclusion of the toroidal field ripple allows us to better reproduce the pitch angle distribution of lost particles when an NTM is present.

The simulated NTM induced losses occur on time scales longer than 100 μs and are composed mainly of trapped particles, consistently with the experimentally observed slow decay of the trapped particles signal after a beam switch-off. A smaller fraction of losses occur also on very short time scales, less than 10 μs, but they do not significantly depend on the NTM presence (*prompt losses*).

The simulated amount of losses depends on the details of radial field perturbation in the region of drift island resonances. In particular, if the radial perturbation is such that the orbits of passing fast ions are stochastic, greater losses are predicted by the simulations. In any case, the qualitative features of the simulated distributions of the toroidal positions, of the pitch angle and of the loss times are similar in both cases.

We conclude that the fast ion losses measured in ASDEX Upgrade are consistent with both the drift islands and the orbit stochasticity mechanisms, the main difference between the two mechanisms being the absolute flux of fast ion losses. As this amount critically depends on the eigenfunction radial profile, more detailed and quantitative simulations would require also a better knowledge of such perturbation profile.

Acknowledgments

The authors are indebted for the material and information received from E. Strumberger, V. Igochine, M. Maraschek, Mathias Reich and Hartmut Zohm and for the discussions they had and the support they found.

This work was supported by the European Communities under the contract of Association between EURATOM/ENEA. The views and opinions expressed herein do not necessarily reflect those of the European Commission.

References

[1] Heidbrink W.W. *et al* 1994 *Nucl. Fusion* **34** 535
[2] Pinches S.D. 2004 *Plasma Phys. Fusion Control.* **46** B187
[3] Herrmann A. 2003 *Fusion Sci. Technol.* **44** 569
[4] Garcia Munoz M. *et al* 2007 *Nucl. Fusion* **47** L10–L15
[5] Garcia Munoz M. *et al* 2008 *Phys. Rev. Lett.* **100** 055005
[6] Darrow D. 1995 *Rev. Sci. Instrum.* **66** 476
[7] Zweben S.J. 1989 *Nucl. Fusion* **29** 825
[8] Isobe M. 1999 *Rev. Sci. Instrum.* **70** 827
[9] Werner A. and Weller A. 2001 *Rev. Sci. Instrum.* **72** 780
[10] Nishiura M. 2004 *Rev. Sci. Instrum.* **75** 3646
[11] Baeumel S. 2004 *Rev. Sci. Instrum.* **75** 3563
[12] Darrow D.S. 2008 *Rev. Sci. Instrum.* **79** 023502
[13] Jimenez-Rey D. *et al* 2008 *Rev. Sci. Instrum.* **79** 093511
[14] Gobbin M. *et al* 2008 *Nucl. Fusion* **48** 075002
[15] Strumberger E. *et al* 2008 *New J. Phys.* **10** 023017
[16] White R.B. and Chance M.S. 1984 *Phys. Fluids* **27** 2455

[17] White R.B. and Zakharov L.E. 2003 *Phys. Plasmas* **10** 573
[18] Hirshman S.P. and Betancourt S. 1991 *J. Comput. Phys.* **96** 99
[19] Carolipio E.M. *et al* 2002 *Nucl. Fusion* **42** 853
[20] Ralf Dux private communication
[21] Lister G.G. 1985 *Technical. Report* Max Planck Institut Fuer Plasmaphysik IPP 4/222
[22] Boozer A.H. and Kuo-Petravich G. 1981 *Phys. Fluids* **24** 851
[23] Trubnikov B.A. 1965 *Rev. Plasma Phys.* **1** 105
[24] Poli E. 2008 *Phys. Plasmas* **15** 032501
[25] Schirmer J. *et al* 2007 *Proc. 34th EPS Conf. on Plasma Physics (Warsaw, Poland, 2007)* vol 31F (ECA) ed P. Gasior and J. Wolowski (Geneva: EPS) CD-ROM P-1.133
[26] White R.B. 2001 *The Theory of Toroidally Confined Plasmas* (London: Imperial College Press) pp 34–42 chapter 2
[27] Gourdon C. 1970 *Programme Optimize de Calculs Numerisque Dans le Configurations Magnetique Toridales* CEN Fontenay aux Roses